NASA Technical Memorandum 84384

Transmission Electron Microscopy Characterization of Microstructural Features in Al-Li-Cu Alloys

M. Avalos-Borja, P.P. Pizzo, and L.A. Larson

October 1983

NASA
National Aeronautics and
Space Administration

NASA Technical Memorandum 84384

Transmission Electron Microscopy Characterization of Microstructural Features in Al-Li-Cu Alloys

M. Avalos-Borja, Stanford/NASA Joint Institute for Surface and Microstructure Research, Ames Research Center, Moffett Field, CA
P. P. Pizzo, Department of Materials Engineering, San Jose State University, San Jose, CA
L. A. Larson, Stanford/NASA Joint Institute for Surface and Microstructure Research, Ames Research Center, Moffett Field, CA

National Aeronautics and Space Administration

Ames Research Center
Moffett Field, California 94035

TRANSMISSION ELECTRON MICROSCOPY CHARACTERIZATION OF MICROSTRUCTURAL FEATURES IN ALUMINUM-LITHIUM-COPPER ALLOYS

M. Avalos-Borja

Stanford/NASA Joint Institute for Surface and Microstructure Research
NASA Ames Research Center, Moffett Field, California 94035 U.S.A.

P. P. Pizzo

Department of Materials Engineering, San Jose State University
San Jose, California 95192 U.S.A.

L. A. Larson

Stanford/NASA Joint Institute for Surface and Microstructure Research
NASA Ames Research Center, Moffett Field, California 94035 U.S.A.

A transmission-electron-microscopy (TEM) examination of aluminum-lithium-copper alloys has been conducted. The principal purpose of this work is to characterize the nature, size, and distribution of stringer particles which result from the powder-metallurgy (P/M) processing of these alloys. Microstructural features associated with the stringer particles are reported that help explain the stress-corrosion susceptibility of the powder-metallurgy-processed Al-Li-Cu alloys. In addition, matrix precipitation events are documented for a variety of heat treatments and process variations. Hot-rolling is observed to significantly alter the nature of matrix precipitation, and the observations are correlated with concomitant mechanical-property variations.

Introduction

Aluminum-lithium alloys have received much attention because of the rather substantial specific strength and specific stiffness advantage they offer over commercial 2000- and 7000-series aluminum alloys (1,2). As an example, if one compares typical properties of the aluminum-lithium-copper alloys of this investigation to AA 7075-T73 aluminum, the following gains are realized: a 24% increase in the stiffness-to-weight ratio; a 14% increase in the strength-to-weight ratio, based on yield strength; and an 18% increase in ultimate tensile strength.

Aqueous chloride-induced stress corrosion (SC) of high-strength aluminum alloys has been a major service problem in the aircraft industry. Since candidate low-density aluminum aerospace alloys may contain chemically active lithium-rich precipitates and compounds, their corrosion and stress-corrosion behaviors are cause for concern. Few corrosion and stress-corrosion data are, however, available for aluminum-lithium alloys (3,4). In the United States, service experience with lithium-bearing, high-strength aluminum alloys is limited to alloy X-2020, an experimental alloy used as wing-skin panels in the RA-5C aircraft (retired in 1979) (2). Because of the potential near-term implementation of advanced aluminum-lithium alloys, an investigation was begun at Ames Research Center to evaluate the environmental durability of these alloys.

The results of the stress-corrosion (SC) study of two powder-metallurgy (P/M) aluminum-lithium-copper alloys are reported in a companion paper at this conference (5). In that study, microstructural features, primarily oxide particles strung along the extrusion direction, were shown to be correlated with pitting and subsequent SC crack initiation. In an effort to investigate the active nature of these sites, transmission-electron-microscopy (TEM) thin-film techniques were employed.

The primary objective of the TEM study was to determine the nature, size, and distribution of stringer particles in P/M-processed Al-2.6%Li-1.4%Cu (the base alloy) and Al-2.6%Li-1.4%CU-1.6%Mg (the magnesium-bearing alloy). In addition, matrix precipitation events were documented for a variety of heat-treatment and process variations so that the character of matrix precipitation could be correlated to property (tensile strength) variations reported earlier (6,7). Concurrent with the TEM investigation, surface analytical techniques of materials analysis such as secondary ion mass spectroscopy (SIMS) and Auger electron spectroscopy (AES) were used in deriving chemical characterizations of the stringer particles. These results are interpreted in terms of the TEM characterization and are reported in a third paper at this conference (8).

Experimental

The nominal composition (wt.%) of the base alloy is 2.6% lithium and 1.4% copper with the remainder being aluminum. The magnesium-bearing alloy has the same lithium and copper contents, but also contains 1.6% magnesium. Both alloys contain about 0.1% zirconium for microstructural stability.

Both alloys were powder-metallurgy processed. Powders were produced by quickly cooling an atomized molten stream of the high-purity Al-Li-Cu alloy in an argon atmosphere; the cooling rate was about 10^3 °C/s. The powder particles were spherical, about 150 μm in diameter. Powders were packed in an AA 6061 aluminum alloy can, vacuum degassed at 500°C for 2 hr, and cold-isostatic pressed to 415 MPa. The billet was then hot-upset at 480°C, and

extruded at 400°C through a 12.7- by 63.5-mm round-corner die. The maximum extrusion ratio was about 10:1.

Some of the extruded bar was further processed by hot-rolling. Both Al-Li-Cu alloys were rolled at about 427°C with the rolls maintained at 177°C. The section thickness was reduced about 5% per pass, and the material was reheated to 427°C after every four passes. In this manner, a 1.5-mm-thick strip was prepared from the original 12.7-mm-thick extruded bar.

The alloys were solution-treated (ST) for 45 min at either 555°C or 515°C in air and then cold water quenched. Base-alloy specimens were aged at either 170°C or 190°C for varying times; the magnesium-bearing alloy specimens were aged at 190°C. Details of the process and heat treatment have been reported elsewhere (7).

Thin specimens suitable for TEM observations were prepared by spark-cutting 3-mm-diam disks from 0.25-mm-thick foils obtained from the flat coupons used in a tensile-properties characterization study (7). The initial thickness of the tensile coupons was 1.5 mm. The 0.25-mm-thick foil from the undeformed grip section was prepared using standard metallographic polishing techniques by removing material equally from both surfaces. Final electropolishing was done using the twin-jet technique in a 70-30% (by volume) methanol-nitric acid electrolyte, at -20°C, and a current density of 0.2 A/cm^2, which corresponds to the polishing region in the current-versus-voltage-polarization curve. Polishing was stopped when a hole formed in the specimen was detected by a light-activated photocell.

Observations were carried out in a Hitachi H-500H electron microscope, operated at 100 kV, and fitted with a liquid-nitrogen-cooled "finger" to reduce specimen contamination. The pressure in the specimen chamber was less than 7×10^{-7} Torr.

The techniques used include bright field (BF), dark field (DF), selected-area diffraction (SAD), and microdiffraction (μD). Microdiffraction was attained by using the condenser and objective pre-field lense in a high-excitation mode to form a beam that was about 10 nm (diameter) on the specimen. In this instance, an optimization of vacuum conditions and large-area pre-irradiation of the specimen were necessary to minimize hydrocarbon contamination, since the illumination beam was a higher current density than that normally used for standard TEM.

Results

The overall appearance of the general microstructure is similar in both extruded alloys regardless of heat treatment. A low-magnification overview of a typical microstructure is shown in Fig. 1. As seen in the scanning-electron-microscope (SEM) image of Fig. 1a, the predominate feature in the microstructure is parallel stringer particles running along a common direction (the extrusion direction). Most often these stringers follow the grain boundaries of the small (~4-μm) recrystallized grains (Fig. 1b); however, in some cases they are found to pierce individual grains. Because these stringer particles appear to play a key role in the SC behavior of the alloys (5), emphasis is placed on characterizing these particles, as well as those precipitates distributed within the matrix material.

Two types of precipitates predominated in the observations of both extruded alloys: (a) a homogeneously precipitated phase identified as δ' by superlattice reflections and by comparison with previous work in this alloy system (9,10) and (b) a heterogeneously precipitated phase which

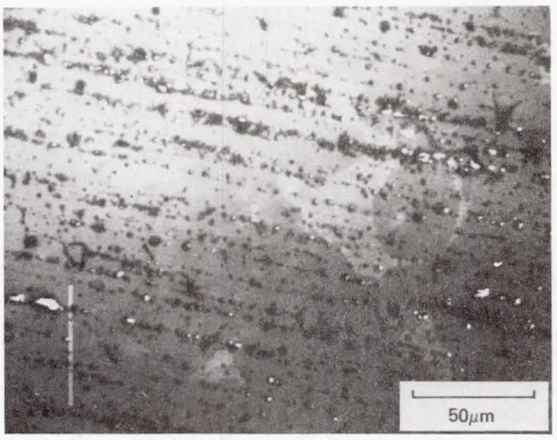

(a)

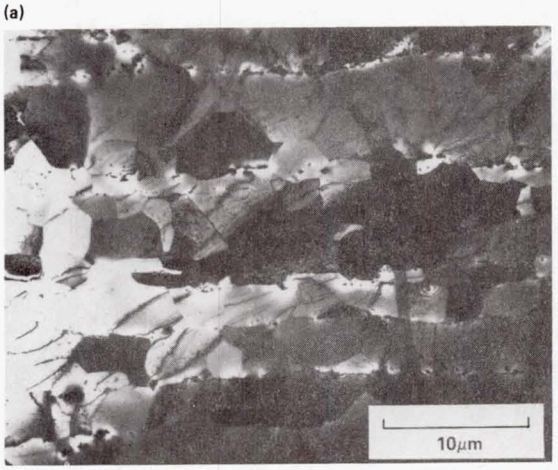

(b)

Figure 1 - General view of alloys used in this study. (a) SEM image; (b) TEM image.

corresponds either to an early stage of T_1 formation (11) or to a different phase, since the diffraction information does not uniquely identify T_1. These precipitation processes occur concurrently during aging, the heterogeneous precipitation exhibiting the slower reaction kinetics. Full identification of the heterogeneous precipitate is in progress. Figure 2 shows these two types of precipitates for the base-alloy solution treated at 515°C and aged for 10 hr at 190°C (peak age). The homogenous δ' precipitates are best seen under the higher contrast conditions of Fig. 2a, and the heterogeneous precipitates are more visible in Fig. 2b.

In the base-alloy solution treated at a higher temperature (ST at 555°C and aged 100 hr at 170°C), the number density of heterogeneous precipitates is increased, as seen in Fig. 3. This higher density is most likely a result of a higher defect density created by quenching from the higher solution-treatment temperature. Also, for these aging conditions, preferential nucleation along low-angle boundaries is observed (Figs. 3b and 3c).

Matrix precipitates in the magnesium-bearing alloy (ST at 515°C and aged 48 hr at 190°C) are shown in Fig. 4. The presence of δ' (Figs. 4c and 4d) and the heterogeneous precipitate (Fig. 4a) is confirmed, the characteristics similar to those observed for the base alloy. Streaks observed in the diffraction pattern (Fig. 4b) are most likely a result of the planar characteristics of the heterogeneous precipitates. At the higher solution-treatment temperature (555°C and aged for 48 hr at 190°C), the number density of heterogeneous precipitates is again increased, as seen in Fig. 5. The extent of this increase appears greater than that observed for the base alloy. Decoration of low-angle boundaries can be seen (Fig. 5a, top) as well.

The microstructure of the extruded and hot-rolled base alloy (ST at 520°C and aged 2.5 hr at 170°C) is shown in Fig. 6. As can be seen by the absence of the superlattice spots (Figs. 6b and 6d), the precipitates do not correspond to δ'. In the extruded and hot-rolled base alloy, precipitation was observed to vary from grain to grain; that is, in some grains precipitates like those shown in Fig. 6a were predominant, whereas in other grains precipitates similar to those in Fig. 6c were noted. However, no other precipitates were observed. These precipitates were identified, based on the diffraction patterns, as originating from Al_5CuLi_3, the R-phase (Fig. 6a), and Al_4Li_9 (Fig. 6c). Although the nonmatrix spots in Fig. 6b may be indexed as the T_1 phase (10), the distance ratio and the angle at which the spots appear match more closely the structure corresponding to the R-phase.

Furthermore, in a ⟨112⟩ matrix zone axis diffraction pattern, no 001 spots were observed, as would be expected from the T_1 structure (10).

In the extruded and hot-rolled magnesium-bearing alloy (ST at 555°C and aged 3 hr at 190°C), a similar suppression of δ' precipitation was observed,

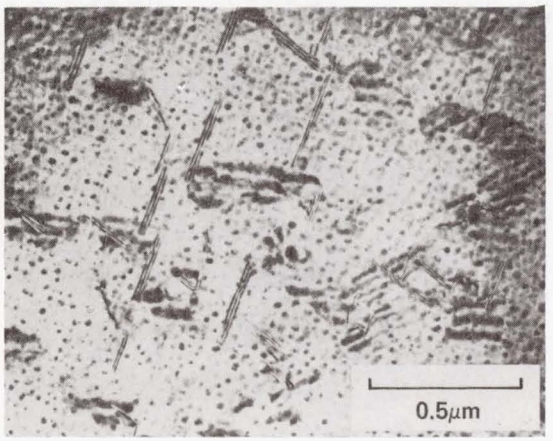

(a)

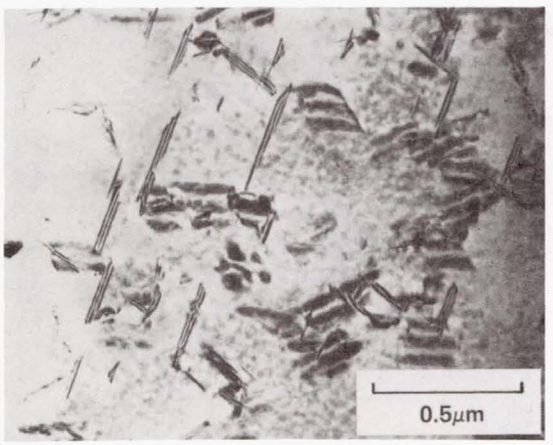

(b)

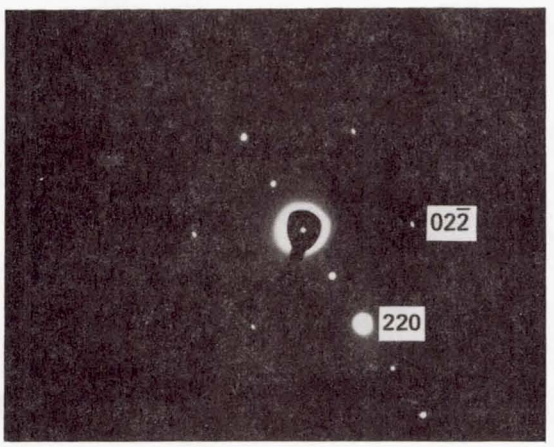

(c)

Figure 2 - Matrix structure of Al-Li-Cu alloy, ST at 515°C, aged for 100 hr at 190°C. Micrographs correspond to two BF images in different diffraction conditions emphasizing homogeneous precipitates in (a), and heterogeneous precipitates in (b); (c) SADP corresponding to (a) and (b).

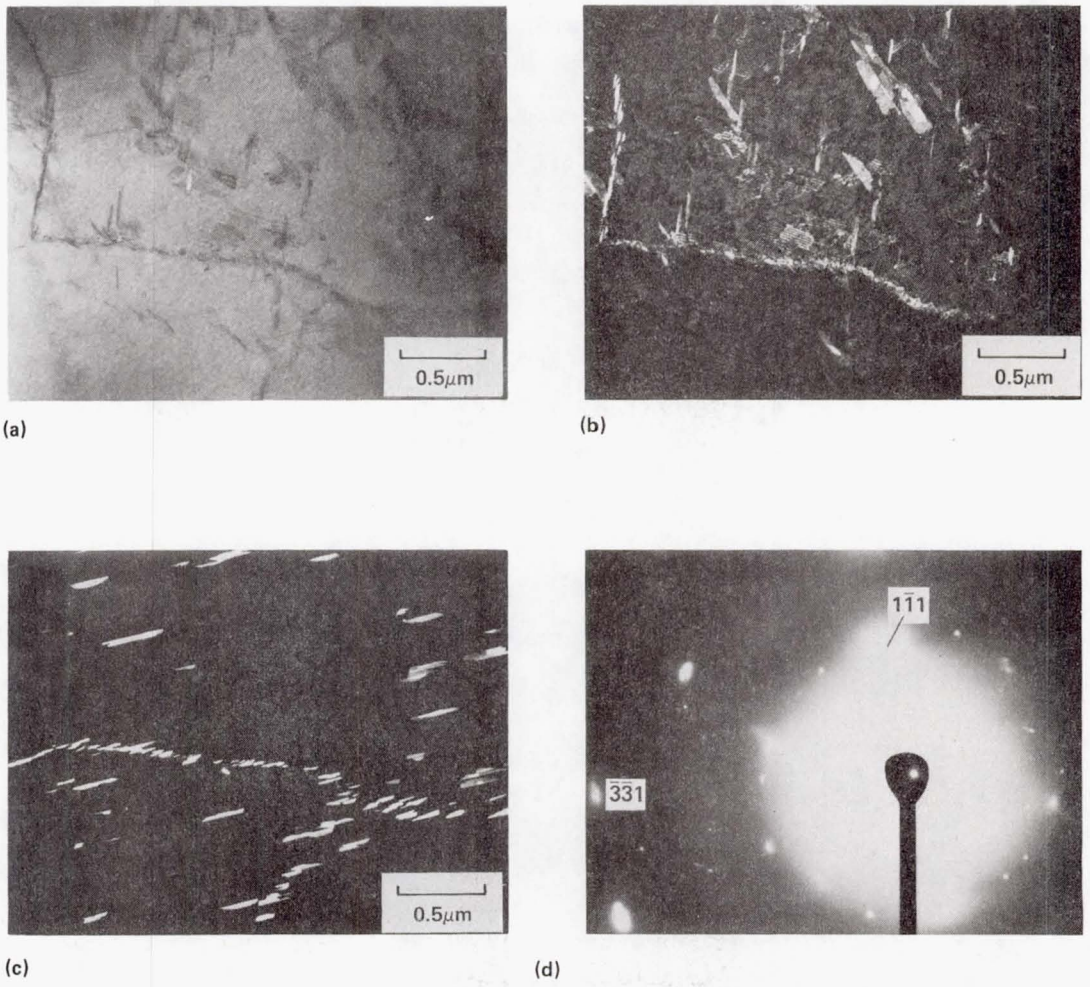

Figure 3 - Microstructure of Al-Li-Cu, ST at 555°C, aged for 100 hr at 170°C; (a) BF; (b) and (c) two DF images showing the planar characteristics of the heterogeneous precipitates, and the decoration of low-angle boundaries; (d) SADP corresponding to (a), (b), and (c).

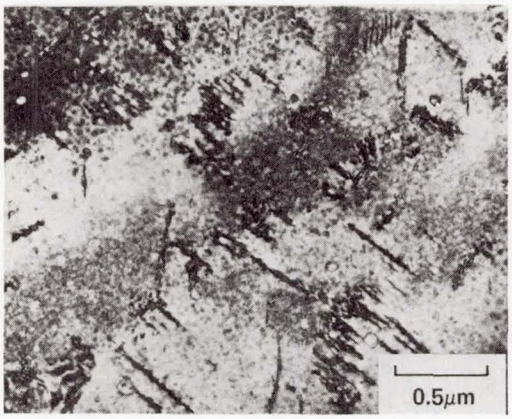

(a)

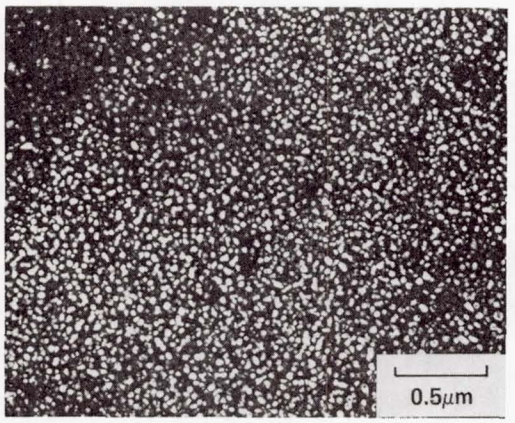

(c)

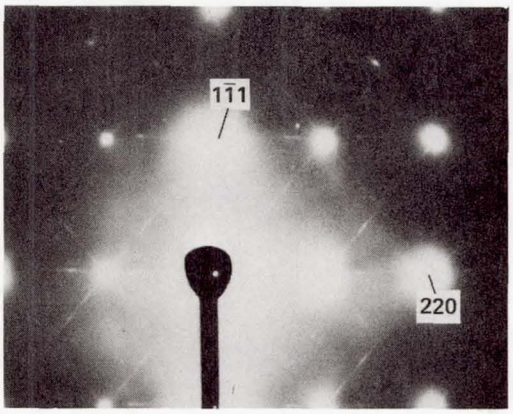

(b)

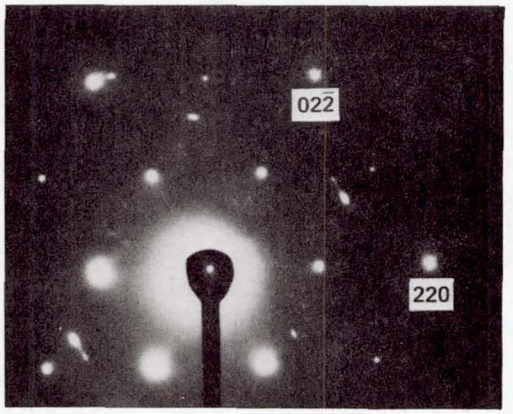

(d)

Figure 4 - Microstructure of Al-Li-Cu-Mg alloy, ST at 515°C, aged for 48 hr at 190°C. (a) BF; (b) SADP corresponding to (a) — note the streaking in the DP owing to the planar precipitates; (c) DF using a superlattice spot, showing size and distribution of δ' precipitates; (d) SADP corresponding to (c).

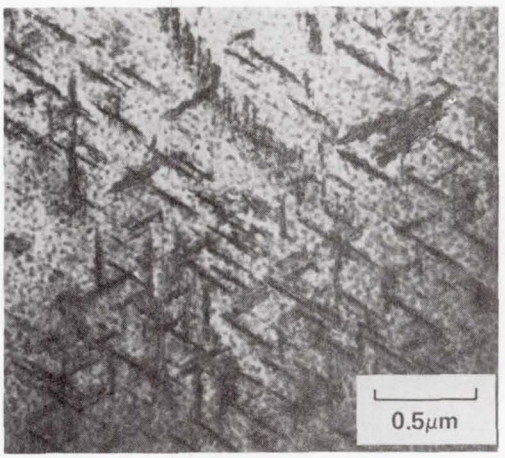

(a)

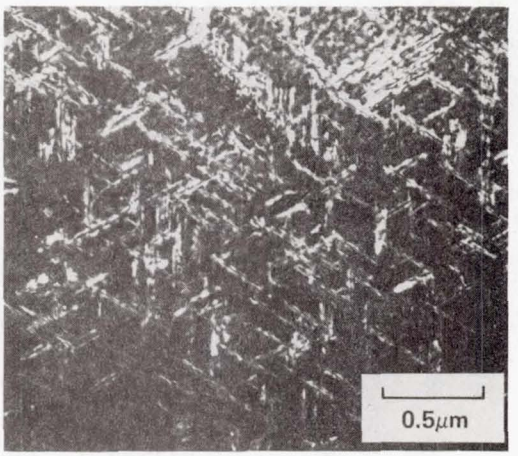

(b)

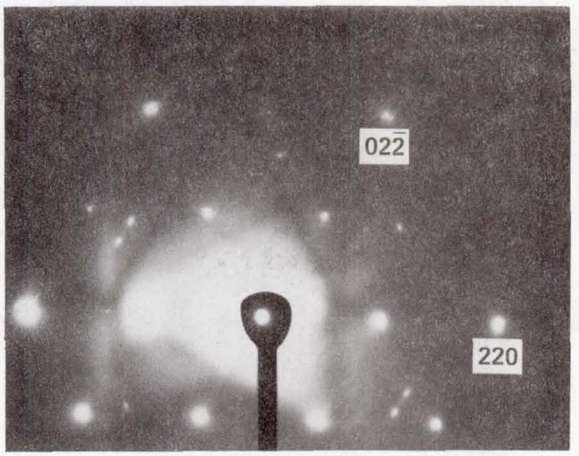

(c)

Figure 5 - Microstructure of Al-Li-Cu-Mg, ST at 555°C, aged for 48 hr at 190°C. (a) BF and (b) DF showing the increase in number density of heterogeneous precipitates upon ST temperature; (c) SADP corresponding to (a) and (b).

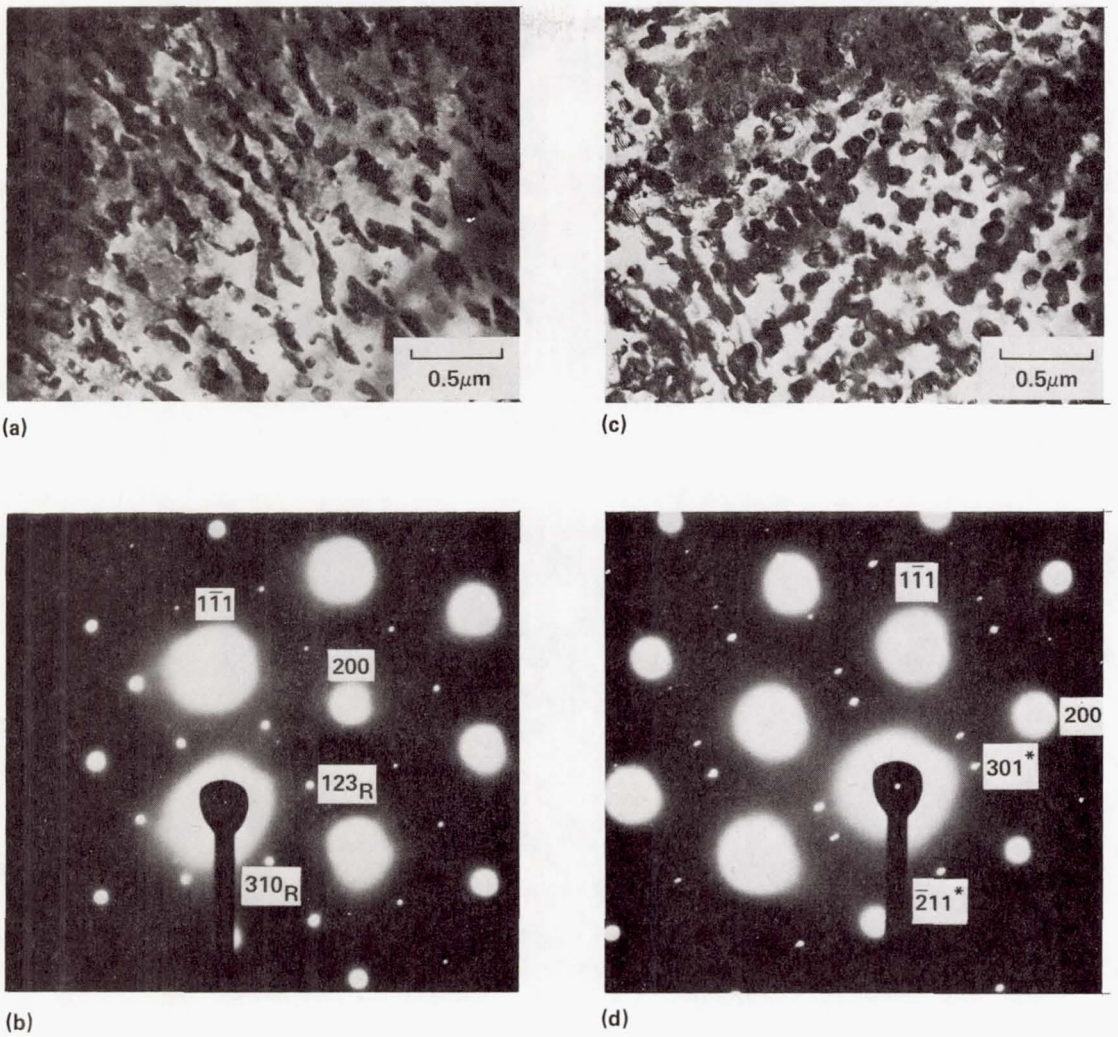

Figure 6 - Microstructure of hot-rolled Al-Li-Cu, ST at 520°C, aged for 2.5 hr at 170°C, showing the formation of large precipitates, (a) and (c), identified tentatively from the diffraction patterns, (b) and (d), as corresponding, respectively, to the Al_5CuLi_3 and Al_4Li_9 phases (indicated by *).

as seen in Fig. 7, where comparison is made between the extruded versus the extruded and hot-rolled conditions (Figs. 7a and 7d vs Figs. 7c and 7d, respectively). In this case, the hot-rolled specimen showed a homogeneous distribution of large precipitates, and very little or none of the "needle-like" heterogeneous precipitates observed in the as-extruded material. Although the large precipitates have not yet been identified, they do not correspond to δ', as can be seen from the absence of superlattice reflections (compare Figs. 7d and Fig. 7b).

The stringer particles found in these powder-metallurgy-processed alloys are shown in Fig. 8. As seen in the TEM close-up, the stringers are composed of three distinct regions that seem to be related in some way. First, there is an almost electron-opaque region (dark feature in Fig. 8a), that is less susceptible to chemical attack by the solution used for electropolishing. Second, a semitransparent, large, rounded region (B in Fig. 8a) is observed that surrounds the darker region and extends into the adjacent grains without any apparent effect on matrix precipitation events. Third, an

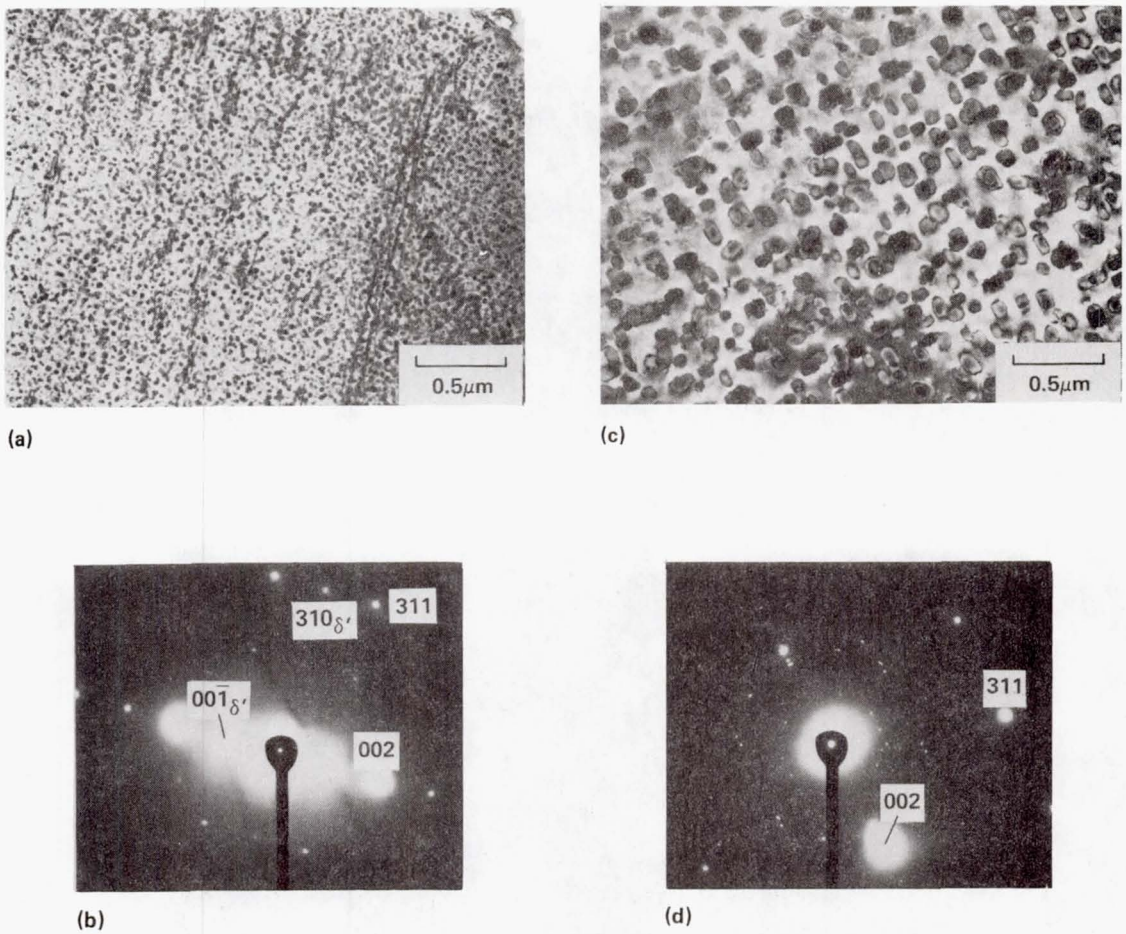

Figure 7 - Microstructure of magnesium-bearing alloy, as extruded (a) and (b), and hot-rolled (c) and (d). Note the absence of δ' superlattice diffraction spots (like 001 and 310) in the hot rolled material.

electron-transparent region (C in Fig. 8a) is present within the semitransparent region and attached to the dark region.

Diffraction information was obtained from selected area diffraction of these regions and results were compared to the matrix. A diffraction pattern from the matrix in grain I (Fig. 8a) is shown in Fig. 8b. When a dark particle (region A, Fig. 8a) is included, no change in the diffraction pattern is observed, verifying the electron opaqueness of the particle. When the semitransparent region (B in Fig. 8a) is included, diffuse scattering occurs, indicating that this region may consist of some amorphous material. When the electron-transparent region (C in Fig. 8c) is included, well-defined rings are observed, indicating the presence of a fine polycrystalline structure.

Further experiments in an area free of the matrix were performed using microdiffraction. In this case a stringer particle located just at the edge of the polishing hole was used (Fig. 9). This allowed diffraction from a much smaller area at the very edge of the otherwise nontransparent particles, with little or no matrix-diffraction interference. Type-A and type-C features were located along the edge, and they are denoted by A' and C' in Fig. 9a. Microdiffraction corresponding to the matrix, the dark particle (A' in Fig. 9a), and the electron transparent region (C' in Fig. 9a) is shown in Figs. 9b, 9c, and 9d, respectively. The dark region produced a well-defined,

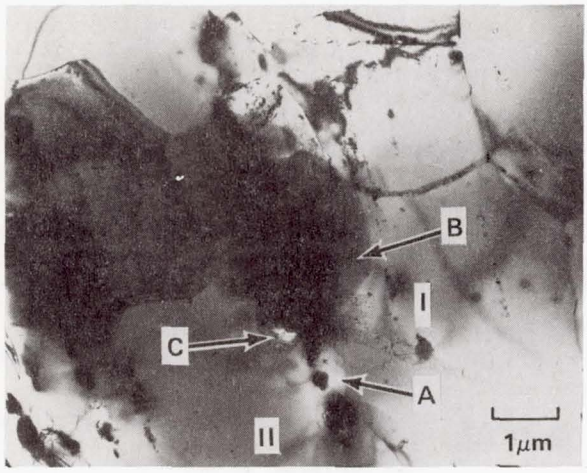

(a)

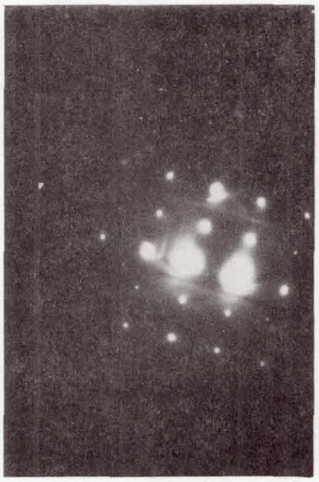

(b)

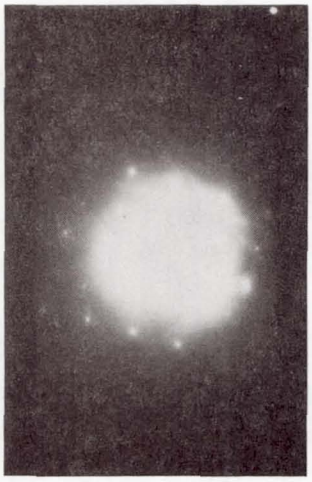

(c)

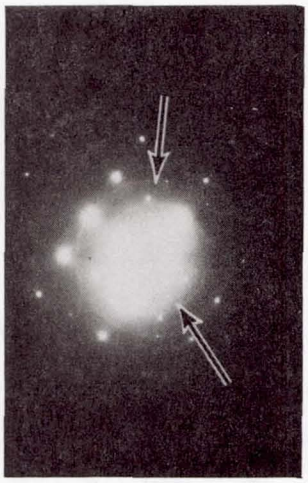

(d)

Figure 8 - Typical components of stringer "particles". (a) A: electron opaque core; B: "carbonaceous cloud" surrounding feature A and extending into neighboring grains; C: associated electron-transparent feature. (b) SADP from matrix only; (c) SADP from matrix plus feature B (note increase in diffuse scattering only); (d) SADP from matrix plus feature C (note additional rings).

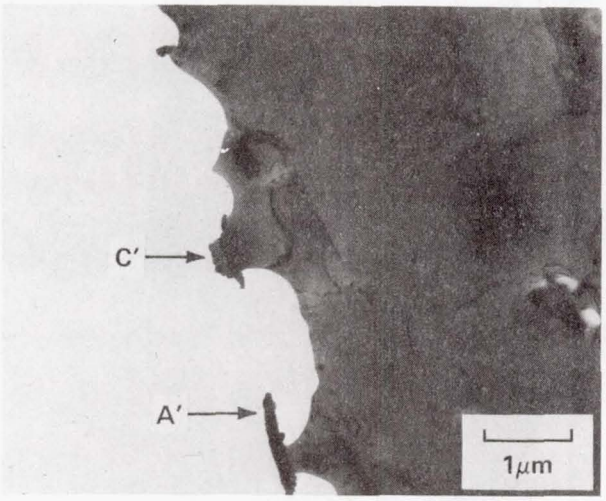

(a)

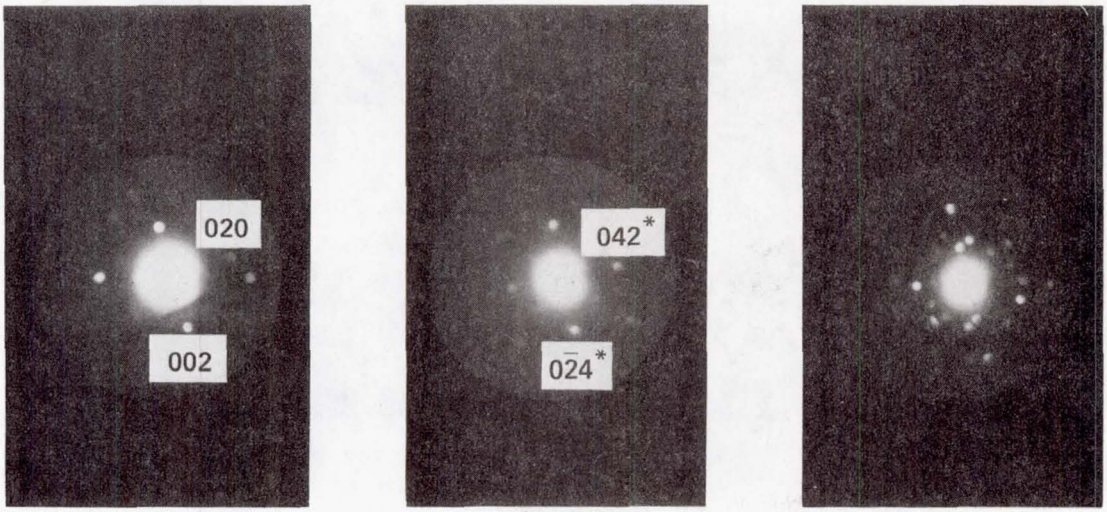

(b) (c) (d)

Figure 9 - Microdiffraction (μD) of free stringer-particle components. (a) BF indicating the location of component A' (similar to A in Fig. 8a), and C' (similar to C in Fig. 8a); (b) μD from matrix; (c) μD from A', indices (*) correspond to L_iC_uO (note single-crystalline character); (d) μD from C' (note polycrystalline structure).

single-crystalline pattern identified as LiCuO, and the transparent region again gave indication of fine polycrystalline structure.

In an attempt to examine the influence of a high-temperature solution treatment on the stringer particles, a base-alloy TEM disk was solution-treated at 610°C for 10 min and cold-water quenched. Subsequent TEM analysis confirmed that the arrays did not dissolve; instead, the stringer particles coarsened.

Discussion

The primary observations from the TEM analysis are as follows:

1. The matrices of the lithium-containing alloys can contain both homogeneous and heterogeneous precipitates. The homogeneous precipitate has been identified as δ'. The identity of the heterogeneous precipitate has not been established, but appears to depend on the chemical content, process history, and heat treatment of the alloys.

2. A high density of stringer particles exists along the extrusion direction in these alloys; the particles are composed of at least three components: an amorphous region, a single-crystal region (tentatively indexed as LiCuO), and a fine polycrystalline region.

The size and distribution of heterogeneous precipitates in the matrices of the extruded alloys is consistent with data reported by other investigators (11,12). However, we have been unable to verify directly, through selected area diffraction, that these precipitates are of the T_1 phase. Our data suggest that the heterogeneous precipitate is either δ' (Al_3Li) or perhaps a precursor step in T_1 formation. A previous investigation on an Al-2.0%Li-2.5%Cu ingot alloy (aged 21 hr at 200°C) has identified heterogeneous precipitate as the T_1 phase (11).

A higher density of heterogeneous precipitates was observed in the matrices with increased solution-treatment temperature (compare Figs. 3a and 3b with Fig. 2b). Additionally, progressive decoration of low-angle boundaries with increasing time at the aging temperature (Figs. 3b, 3c, and 5) occurred. These observations are as would be expected. Quenching from the higher solution-treatment temperature will result in a higher defect density in the matrix, and a higher defect density should correspond to a greater number of nucleation sites for the heterogeneous precipitation reaction. The low-angle boundaries would be expected to act as preferential nucleation sites as well. The plate-like character of the heterogeneous precipitates in the magnesium-bearing alloy is clearly indicated by streaking in the selected-area-diffraction pattern (Fig. 4c) and becomes more prominent with longer aging times. The plate-like character of the heterogeneous precipitates is distinctly different in the base alloy (compare Figs. 2b and 3b) and streaking is not observed (Fig. 2c), which suggests a different precipitate morphology.

Although the strength in these Al-Li-Cu alloys can be assumed to be a function primarily of the nature, size, and interparticle spacing of the homogeneous (δ') matrix precipitates, a component of strength may be expected from the heterogeneous precipitate as well. This correlates with an increase of flow strength (about 8%) reported earlier (7) for the 555°C versus 520°C solution-treatment conditions in the magnesium-bearing alloy over a range of aging times, and reflects both the plate-like character of the precipitate and increased density. The flow strength of the base alloy was found to be relatively insensitive to solution-treatment temperature and, thus, is in qualitative agreement with the configuration of the precipitate and the lesser influence of solution-treatment temperature on the number density.

The size and distribution of stringer particles observed in the alloys (Figs. 1a and 1b) appears to determine the recrystallized grain size. This suggests that the 0.1% zirconium addition to these P/M alloys was insufficient to retard recrystallization and grain growth which occurred during the solution-treatment of the extruded materials and of the materials that were extruded and hot-rolled.

The stringer particles are complex and appear to be made up of at least three components (Figs. 8 and 9). Data from SIMS and AES strongly suggest a high lithium content (8), and these stringers clearly play an active role in determining the aqueous-chloride stress-corrosion behavior of the alloys (5). Since the major component of the stringer particles (region A, Fig. 8a) seems unaffected by the electropolishing solution, it is rationalized that the active nature of the stringers is more associated with the companion particles (regions B and C, Fig. 8a).

The exact nature and composition of the three components of the stringers remains to be determined. It is possible that the lithium-rich γ-phase, Li_2Al, or the δ-phase, AlLi, may be present in these arrays. There are other possibilities, however, such as thermodynamically stable ceramic phases (13); oxides of aluminum, lithium, and copper; or trace impurities (Na, K, Ca, Zr) in the alloys.

The observation that the stringer particles are lithium-rich is significant. If the lithium that contains gross stringer particles becomes unstable at some point in the processing of the alloy, lithium-rich companion phases could form (such as regions B and C, Fig. 8a); this could explain the active electrochemical behavior of the stringers.

The extruded and hot-rolled alloys have been found to exhibit a significant reduction in strength (6). Specifically, it has been shown that relative to the extruded plate for a given heat treatment the yield and ultimate strength of the base alloy is reduced by about 9% when it is hot-rolled. The magnesium-bearing alloy exhibited greater than a 30% reduction in flow strength from hot-rolling with no apparent loss in either lithium or magnesium content.

From a comparison of the matrix precipitates in the extruded and hot-rolled versus the extruded alloys (compare Fig. 6b with Fig. 2a and compare Fig. 7b with Fig. 4b) and the chemical characterization work (8), it is rationalized that hot-rolling results in the rapid nucleation and growth of lithium-rich phases such as Al_5CuLi_3 and Al_4Li_9. These phases are stable at the hot-rolling temperature (427°C) and apparently do not re-dissolve with subsequent heat treatment of the alloys. Thus, solution and aging treatments performed subsequent to hot-rolling were ineffective in producing δ'. The reduced strength of the hot-rolled material was due to the loss of the δ' matrix precipitate.

Conclusions

The microstructural state of powder-metallurgy-processed Al-Li-Cu alloys is complex and dependent on consolidation, process, and heat-treatment steps. Lithium can segregate to the oxide stringer particles, which are usually present, and promote complex interactions with the various elements present in the matrix or the environment. In this manner, active sites may be created that adversely affect the stress-corrosion behavior in aqueous sodium-chloride solution.

Extruded and hot-rolled Al-Li-Cu may not precipitate δ' particles; instead, Al_5CuLi_3 and Al_4Li_9 precipates are formed, thus reducing the flow strength relative to that of the extruded material where δ' formation is the primary precipitation event.

References

1. T. H. Sanders, Jr. and E. S. Balmuth, Metallurgical Progress, 113 (1978), p. 32.

2. E. S. Balmuth and R. Schmidt, Aluminum-Lithium Alloys, T. H. Sanders, Jr. and E. A. Starke, Jr., eds., AIME, 1981, p. 69.

3. J. U. Evancho, Final Technical Report (Feb. 8, 1973-Feb. 7, 1974), Naval Air Development Center Contract N62269-73-C-0219, June 1974.

4. P. Niskanen, T. H. Sanders, Jr., J. G. Rinker, and M. Marek, Corrosion Science, 22 (4) (1982) p. 283.

5. P. P. Pizzo, R. P. Galvin and H. G. Nelson, Aluminum-Lithium Alloys, T. H. Sanders, Jr. and E. A. Starke, Jr., eds., AIME, 1983.

6. P. P. Pizzo, NASA CR-166339, 1980.

7. P. P. Pizzo, NASA CR-3578, 1982.

8. L. A. Larson, P. P. Pizzo, and M. Avalos-Borja, Aluminum-Lithium Alloys, T. H. Sanders, Jr. and E. A. Starke, Jr., eds., AIME, 1983.

9. D. B. Williams and J. N. Edington, Metal Science, 9 (1975) p. 529.

10. B. Noble and G. E. Thompson, Metal Science Journal, 5 (1971) p. 114.

11. B. Noble and G. E. Thomspon, Metal Science Journal, 6 (1972) p. 167.

12. F. S. Lin, S. B. Chakrabortty, and E. A. Starke, Jr., Metallurgical Transactions A, 13A (1982) p. 401.

13. E. M. Levin, C. R. Robbins, and H. F. McMurdie, Phase Diagrams for Ceramists, M. K. Reser, ed., The American Ceramic Society, Columbus, Ohio, 1964.

1. Report No.	2. Government Accession No.	3. Recipient's Catalog No.
NASA TM 84384		

4. Title and Subtitle	5. Report Date
TRANSMISSION ELECTRON MICROSCOPY CHARACTERIZATION OF MICROSTRUCTURAL FEATURES OF AL-LI-CU ALLOYS	October 1983
	6. Performing Organization Code

7. Author(s)	8. Performing Organization Report No.
M. Avalos-Borja, P. P. Pizzo,* and L. A. Larson	A-9407
	10. Work Unit No. T-4241

9. Performing Organization Name and Address	11. Contract or Grant No.
Stanford/NASA Joint Institute for Surface and Microstructure Research, Ames Research Center, Moffett Field, CA and *San Jose State University, Department of Materials Engineering, San Jose, CA	

12. Sponsoring Agency Name and Address	13. Type of Report and Period Covered
National Aeronautics and Space Administration Washington, D.C. 20546	Technical Memorandum
	14. Sponsoring Agency Code 505-33-21

15. Supplementary Notes

Point of Contact: Patrick P. Pizzo, Associate Professor, Department of Materials Engineering, San Jose State University, San Jose, CA 95192 (408) 277-2436 or (408) 277-2446

16. Abstract

A transmission-electron-microscopy (TEM) examination of aluminum-lithium-copper alloys has been conducted. The principal purpose of this work is to characterize the nature, size, and distribution of stringer particles which result from the powder-metallurgy (P/M) processing of these alloys. Microstructural features associated with the stringer particles are reported that help explain the stress-corrosion susceptibility of the powder-metallurgy-processed Al-Li-Cu alloys. In addition, matrix precipitation events are documented for a variety of heat treatments and process variations. Hot-rolling is observed to significantly alter the nature of matrix precipitation, and the observations are correlated with concomitant mechanical-property variations.

17. Key Words (Suggested by Author(s))	18. Distribution Statement
Aluminum-lithium alloys Transmission electromicroscopy Micro-diffraction Precipitation	Unlimited Subject Category: 26

19. Security Classif. (of this report)	20. Security Classif. (of this page)	21. No. of Pages	22. Price*
Unclassified	Unclassified	18	A01

*For sale by the National Technical Information Service, Springfield, Virginia 22161